






Open Archive Toulouse Archive Ouverte (OATAO)

OATAO is an open access repository that collects the work of Toulouse researchers and makes it freely available over the web where possible

This is an author's version published in: <http://oatao.univ-toulouse.fr/27427>



Official URL: <https://doi.org/10.1088/1361-6528/ab55c3>

To cite this version:

Sábio, Rafael Miguel  and Santagneli, Silvia Helena and Gressier, Marie 
and Caiut, José Maurício Almeida and Pazin, Wallance Moreira and Leite,
Ilaiali Souza and Inada, Natalia Mayumi and Rosa da Silva, Robson and
Ribeiro, Sidney José Lima and Menu, Marie-Joëlle  *Luminescent
nanohybrids based on silica and silylated Ru(II)—Yb(III) heterobinuclear
complex: new tools for biological media analysis.* (2019) *Nanotechnology*,
31 (8). 085709. ISSN 0957-4484

Any correspondence concerning this service should be sent
to the repository administrator: tech-oatao@listes-diff.inp-toulouse.fr

Luminescent nanohybrids based on silica and silylated Ru(II)—Yb(III) heterobinuclear complex: new tools for biological media analysis

Rafael Miguel Sábio^{1,2} , Silvia Helena Santagneli¹, Marie Gressier², José Maurício Almeida Caiut³, Wallance Moreira Pazin⁴, Ilaiali Souza Leite⁵, Natalia Mayumi Inada⁵, Robson Rosa da Silva⁵ , Sidney José Lima Ribeiro¹ and Marie-Joëlle Menu²

¹ Institute of Chemistry, São Paulo State University, UNESP, CP355 Araraquara SP, Brazil

² CIRIMAT Université de Toulouse, CNRS, INPT, UPS, Toulouse, France. 118 route de Narbonne, F 31062, Toulouse Cedex 9, France

³ Departamento de Química, Faculdade de Filosofia, Ciências e Letras de Ribeirão Preto, Universidade de São Paulo, 14040 901 Ribeirão Preto, SP, Brazil

⁴ Departamento de Física, Faculdade de Filosofia, Ciências e Letras de Ribeirão Preto, Universidade de São Paulo, 14040 901 Ribeirão Preto, SP, Brazil

⁵ São Carlos Institute of Physics, University of São Paulo, São Carlos, SP, Brazil

E mail: rafaelmsabio@gmail.com

Abstract

Lanthanide (Ln) complexes emitting in the near-infrared (NIR) region have fostered great interest as upcoming optical tags owing to their high spatial and temporal resolution emission as well deeper light penetration in biological tissues for non-invasive monitoring. For use in live-cell imaging, lanthanide complexes with long-wavelength absorption and good brightness are especially critical. Light-harvesting ligands of Ln complexes are typically excited in the ultraviolet region, which in turn trigger simultaneously autofluorescence and long-exposition damage of living systems. The association of d-metalloligands rather than organic chromophores enables the excitation of NIR-emitting Ln complex occurs in the visible region. Taking advantage of the long-lived excited states and intense absorption band in the ultraviolet (UV) to NIR region of Ru(II), we successfully design a dual-emitting (in the visible and NIR region) *d f* heterobinuclear complex based on Ru(II) metalloligand and Yb(III) complex. In addition, we developed luminescent nanohybrids by grafting of Ru(II) Yb(III) heterobinuclear complexes containing silylated ligands on the surface of mesoporous and dense silica matrix. The nanomarkers were successfully applied for imaging of murine melanoma B16-F10 and neonatal human dermal fibroblast HDFn cell cultures by one-photon or two-photon absorption using laser scanning confocal microscopy. Great cellular uptake, low cytotoxicity and the possibility to achieve visible and NIR emission via two-photons excitation show that the nanohybrids are remarkable markers for *in vitro* and a potential tool for *in vivo* applications.

Supplementary material for this article is available [online](#)

Keywords: silylated *d f* heterobinuclear complexes, grafting trialkoxysilyl group, mesoporous silica nanoparticles, visible and NIR luminescent nanohybrids, luminescent nanomarkers

(Some figures may appear in colour only in the online journal)

1. Introduction

Fluorescence imaging has become the preferred minimally invasive clinical technique for diagnosis and therapy enabling the real time detection of biomarkers through millimeters below the tissue surface with high spatial resolution mapping. Conventional wide-field fluorescence microscopy can provide submicron spatial resolution of fluorescent probes within living cells, but is frequently limited in sensitivity and spatial resolution by cell autofluorescence background, light scattering and out-of-focus in the visible region. Fluorescence imaging at near-infrared (NIR) wavelengths minimizes autofluorescence and increase imaging depth. Therefore, NIR fluorescent probes have been developed as alternatives to traditional visible fluorophores for imaging molecular processes across spatial scales ranging from cells and tissues to living organisms. The NIR luminescence can not only permeate into deeper tissues with minimal light attenuation by the biological matrix, but also avoid the cell autofluorescence that hinders the evaluation of target signal (mostly in the ultraviolet visible region). Among several fluorescence imaging techniques, laser scanning confocal microscopy (LSCM) directly allow for excitation and detection of NIR fluorescence offering micron-scale resolution at sharply defined optical sections, and autofluorescence-free imaging approach with intrinsic depth. However, nanoprobe with NIR-incoming-NIR-outgoing fluorescence features are still scarce.

NIR-emitting lanthanide complexes (contrasting agent) have garnered considerable attention in biomedical applications due to their milliseconds regime emission lifetimes and sharp emission bands in the biological transparency window (700–1000 nm) [1, 2]. However, a recurrent problematic in NIR-emitting lanthanide complexes consists on the excitation wavelength choice, usually excited in UV region [3, 4]. One of the strategies to overcome these limitations consists on the rationally design of *d f* heterobinuclear compounds by the association of NIR-emitting lanthanide complex with *d*-metalloligands compounds.

Specifically, ruthenium(II) polypyridyl metalloligands show strong visible light absorption via metal-to-ligand charge transfer (MLCT) transitions. Their long-lived excited states (often of triplet metal-to-ligand charge-transfer (³MLCT)) reachable through one (OPA) and two-photon absorption (TPA) [5–7] that may be efficient sensitizers for the low energy *f f* excited states of NIR-emitting Yb(III), Nd(III), Er(III) ions [8–11]. Wei *et al* [12] have described a novel NIR luminescent binuclear complex for the detection of alpha-fetal protein in human serum samples based on quenching the NIR emission intensity of the Ru–Nd complex. Although good results were achieved in simulated biological media, this heterobinuclear complex was sensitized by one-photon excitation at 468 nm, which is out of the region of high transparency for biological tissues.

Seeking to explore the potential of the *d f* heterobinuclear complexes for long-term fluorescence imaging, it is rational to design new strategies in order to immobilize them in biocompatible and inert host particles. Mesoporous silica nanoparticles (MSNs) have been extensively investigated as

host for immobilization of drugs and luminescent probes. Once the luminescent probes are loaded inside the pores, MSNs can prevent their premature release, degradation and deactivation effects before reaching their designated target [13–15]. MSNs are biocompatible and biodegradable nano-platforms possessing tailorable particle and pore sizes besides silanol groups available for further grafting reactions [13–15]. The inner and outer porous surface can be easily modified with functional chemical groups at mild conditions [15].

Herein, we proposed the visible/NIR-incoming-NIR-outgoing fluorescent *d f* heterobinuclear complexes modified with the silylated ligands immobilized by covalent binding on the surface of MSNs. This approach prevents nonhomogeneous embedding and leaching of luminescent probe from host matrix [16, 17]. In our previous work [18, 19], bipyridine and diketone derivative ligands such as bpy-Si and TTA-Si appropriately substituted by a trialkoxysilyl groups were successfully isolated and used to synthesize silylated *d f* heterobinuclear complexes. Previously, we have described the synthesis of highly luminescent silylated [Eu(TTA-Si)₃] and [Eu(TTA)₃(bpy-Si)] complexes grafted onto mesoporous and dense silica nanoparticles [17, 20]. We also showed that [Ru(bpy)₂(bpy-Si)]Cl₂ complexes grafted inside dense SiO₂ nanoparticles have succeeded as optical tag [21, 22] for fluorescent imaging of *Pseudomonas aeruginosa* biofilms [22].

This work shows the successful synthesis of [Yb(TTA)₃(bpmd)Ru(bpy)(bpy-Si)]Cl₂ (labeled RuL² YbL⁴) heterobinuclear complex, bearing the alkoxysilyl group on bipyridine ruthenium(II) moiety and the fabrication of two new luminescent silica-based nanohybrids. Both nanohybrids were designed by RuL² YbL⁴ grafting onto mesoporous or dense silica surface labeled SiO₂-RuL² YbL⁴ and SiO₂-d-RuL² YbL⁴, respectively. Luminescence properties of these nanohybrids are examined and compared to the corresponding free RuL² YbL⁴ complex. These nanohybrids are displayed as new dual-emitting (in the visible and NIR region) nano-platform for bioanalysis. To the best of our knowledge, there are still no reports disclosing the fabrication of SiO₂-RuL² YbL⁴ nanohybrid for luminescent *in vitro* imaging of healthy and cancer cells achieved by OPA or TPA using LSCM. Low cytotoxicity and the possibility to obtain visible and NIR emission via two-photons excitation suggests the RuL² YbL⁴ nanohybrid as a potential tool for *in vivo* applications.

2. Experimental

2.1. Materials

All reagents were purchased from Acros, Aldrich, SDS, New Biochem, Fluka, or Quimis and were used as received. The RuL² YbL⁴ heterobinuclear complex was synthesized and fully characterized as described in support information. Ludox AS40 (Aldrich) was used as dense silica nanoparticles (labeled DSNs). DSNs contains 40 wt% SiO₂, with an average particle size of 24 ± 2 nm, and the specific surface area (*S*_{BET}) of 138 m² g⁻¹. Spherical mesoporous SiO₂ nanoparticles (labeled

MSNs) were obtained as protocol described by Nandiyanto *et al* [23]. MSNs with an average size of 47 ± 5 nm, a specific surface area value (S_{BET}) of $675 \text{ m}^2 \text{ g}^{-1}$ and average pore size of 9 nm were obtained and displayed in support information. Dichloromethane and ethanol were purified by distillation in an inert atmosphere before use. The Schlenk system was used to prevent the hydrolysis reaction of the alkoxy silyl groups in the grafting reactions.

Murine melanoma (B16-F10, catalog number CRL-6475) and neonatal human dermal fibroblast (HDFn, catalog number C0045C) cell lines were purchased from the American Type Culture Collection (USA) and Thermo Fischer Scientific (USA), respectively. Both cells were cultivated with Dulbecco's Modified Eagle's Medium (DMEM, Cultilab, Brazil) supplemented with 10% (v.v⁻¹) fetal bovine serum (FBS, Cultilab, Brazil) in humidified incubator at 37 °C under 5% CO₂ atmosphere. MTT (3-[4,5-dimethylthiazol-2-yl]-2,5-diphenyltetrazolium bromide) was purchased from Sigma-Aldrich (USA) and dimethyl sulfoxide (DMSO) from Labsynth (Brazil).

2.2. Characterization

DRIFT spectra were obtained in the spectral range from 4000 to 400 cm⁻¹ with a Perkin-Elmer 1760 X (DTGS detector) spectrometer. Elemental analyses of C, H, N and S were performed on a Fisons EA1108 Instrument CHNS/O elemental analyzer. Nitrogen and Sulfur contents allow the determination of the grafting efficiencies, R, expressed in millimoles of complex per gram of silica. Particle shape and size were examined via FEG-SEM, using a JEOL JSM 6700F microscope. A drop of sol was diluted in ethanol. The samples were not metallized. The presence of ytterbium and ruthenium DSNs and MSNs were evaluated by Scanning and Transmission Electron Microscopy (STEM), using a JEOL JEM-ARM200F Cold FEG EDS/EELS microscope. A drop of sol was diluted in ethanol. A carbon-coated grid was dipped in the solution and allowed to air-dry at room temperature. The microscopy measurements were carried out in the Raimond Castaing-UMS 3623 microcharacterization center. ²⁹Si{¹H}CP-MAS and ¹³C{¹H}CP-MAS spectra were obtained on a Ascend III 400WB HD spectrometer, operating at 9.4 T, using a commercial 4mm double resonance MAS-NMR probe. The frequencies of nuclei are 400.13, 79.49 and 100.6 MHz for ¹H, ²⁹Si and ¹³C and spinning speeds of 15 and 10 kHz, respectively. ²⁹Si{¹H}CP-MAS spectra were measured with ¹H 90° pulse length of 2.9 μs, a contact time of 2.5 ms, and a relaxation delay of 5 s. ¹³C{¹H}CP-MAS spectra were measured with ¹H 90° pulse length of 3.1 μs, a contact time of 3.5 ms, and a relaxation delay of 5 s. All spectra were acquired with TPPM proton decoupling during the data acquisition applying decoupling pulses of 5.8 μs length (π pulses). Chemical shifts are reported relative to TMS. Luminescence spectra were measured at room temperature using a Jobin-Yvon Model Fluorolog FL3 22 spectrometer equipped with a H10330 75 Hamamatsu detector, TE: cooled NIR-photomultiplier module and a 450 W Xe excitation lamp. Excitation and emission spectra

were recorded under CW excitation and were corrected with respect to the Xe Lamp intensity and spectrometer response.

2.3. Synthesis

Two luminescent nanohybrids were obtained when RuL² YbL⁴ silylated complex was reacted with MSNs (labeled MSNs) and dense silica nanoparticles (Ludox AS40, labeled DSNs). The different nanohybrids were noted as SiO₂-RuL² YbL⁴ and SiO₂ d- RuL² YbL⁴. All nanohybrids are chemically stable for months.

SiO₂-RuL² YbL⁴ nanohybrid: 0.14 mmol (240 mg) of RuL² YbL⁴ complex were dissolved in 20 ml of ethanol/dichlorometane (1:1) and reacted with (415 mg) of MSNs. The mixtures were stirred for 72 h at 295 K in an N₂ atmosphere. The resulting suspensions were dialyzed for 72 h, and the solids were isolated by centrifugation at 15 000 rpm for 15 min. The obtained solids were washed with water, ethanol, dichloromethane, and diethyl ether and then dried under vacuum for 4 h. Elemental analysis %, found (calcd): $R_{\text{Ru}} = 0.13 \text{ mmol g}^{-1}$ and $R_{\text{Yb}} = 0.13 \text{ mmol g}^{-1}$; C, 13.58 (9.76); H, 1.77 (0.80); N, 1.63 (1.63); S, 1.24 (1.24).

SiO₂d-RuL² YbL⁴ nanohybrid. 0.06 mmol (105 mg) of RuL² YbL⁴ complex was dissolved in 20 ml of ethanol/dichlorometane (1:1) and reacted with Ludox silica sol 1.40 g that is 0.56 g of SiO₂. The mixtures were stirred for 72 h at 295 K in N₂ atmosphere. The resulting suspensions were dialyzed for 72 h, and the solids were isolated by centrifugation at 15 000 rpm for 15 min. The solids obtained were washed with water, ethanol, and diethyl ether and then dried under vacuum for 4 h. Elemental analysis %, found (calcd): $R_{\text{Ru}} = 0.04 \text{ mmol g}^{-1}$ and $R_{\text{Yb}} = 0.04 \text{ mmol g}^{-1}$; C, 6.19 (4.20); H, 1.03 (0.35); N, 0.70 (0.70); S, 0.36 (0.53).

2.4. Cytotoxicity assays

To assess SiO₂-RuL² YbL⁴ effects on cellular viability, monolayer cultures of healthy and tumor cells were exposed to the nanoparticles. 96-well plates were seeded with DMEM supplemented with 10% FBS containing 5×10^4 cells ml⁻¹ 24 h prior exposure to the samples. Cells were inoculated with nanoparticles solutions of 50 250 μg ml⁻¹, prepared immediately before their use (using an ultrasonic bath Soni-Tech, Brazil to redisperse the nanoparticles and avoid aggregation) in phenol red-free DMEM supplemented with 10% FBS, and incubated for 24 and 48 h in humidified incubator at 37 °C under 5% CO₂ atmosphere. Cell viability was obtained indirectly by the MTT assay: absorbance was measured at 570 nm with the microplate spectrophotometer Multiskan™ Go (ThermoFisher Scientific, USA) and viability percentages were calculated based on the absorbance values of the control group (cells that were not exposed to nanoparticles).

2.5. Nanohybrid internalization

LSCM was performed to observe the internalization of SiO₂-RuL² YbL⁴ nanohybrid. B16-F10 and HDFn cells were seeded at a density of 10^5 cells ml⁻¹ in CELLview™

Dishes (Greiner Bio-One, Austria) and incubated in 2 ml of phenol red-free DMEM supplemented with 10% FBS for 24 h at 37 °C. Cell media were replaced with nanohybrids solutions of 50 and 250TM g ml⁻¹ and cells were incubated for 24 and 48 h. Samples were gently washed twice with PBS for confocal imaging with the inverted Zeiss LSM 780 laser scanning confocal microscope (Carl Zeiss, Germany) using single-photon (458 nm argon laser excitation with emission collected in 640 nm) and two-photon (Ti-Sapphire laser emitting 900 nm, fluorescence was observed in 480 nm) excitation of SiO₂-RuL² YbL⁴ nanohybrid. To confirm the nanohybrid uptake, B16-F10 and HDFn cell suspensions were analyzed with the flow cytometer Accuri C6 Plus (Becton Dickinson, USA) after 50 and 250 μg ml⁻¹ solutions were incubated for 24 and 48 h. Samples were irradiated with 488 nm laser and fluorescence was collected using a 670 LP filter. Proper gates were made using a negative sample, and data was expressed as fluorescence intensity. For all conditions, 5000 events were analyzed.

2.6. Statistical analysis

Cytotoxicity assay data is expressed as percentages, as mean ± standard deviation. Experiments were repeated in two different occasions, with quintuplicate of each group (total *n* = 10). For statistical analysis, treated groups were compared to the control with the one-way analysis of variance (ANOVA) followed by Tukey's multiple comparison test, performed with GraphPad Prism 5. Statistically significant differences between samples were determined by comparisons presenting *p* ≤ 0.05.

3. Results and discussion

3.1. Fabrication of luminescent silica-based nanohybrids

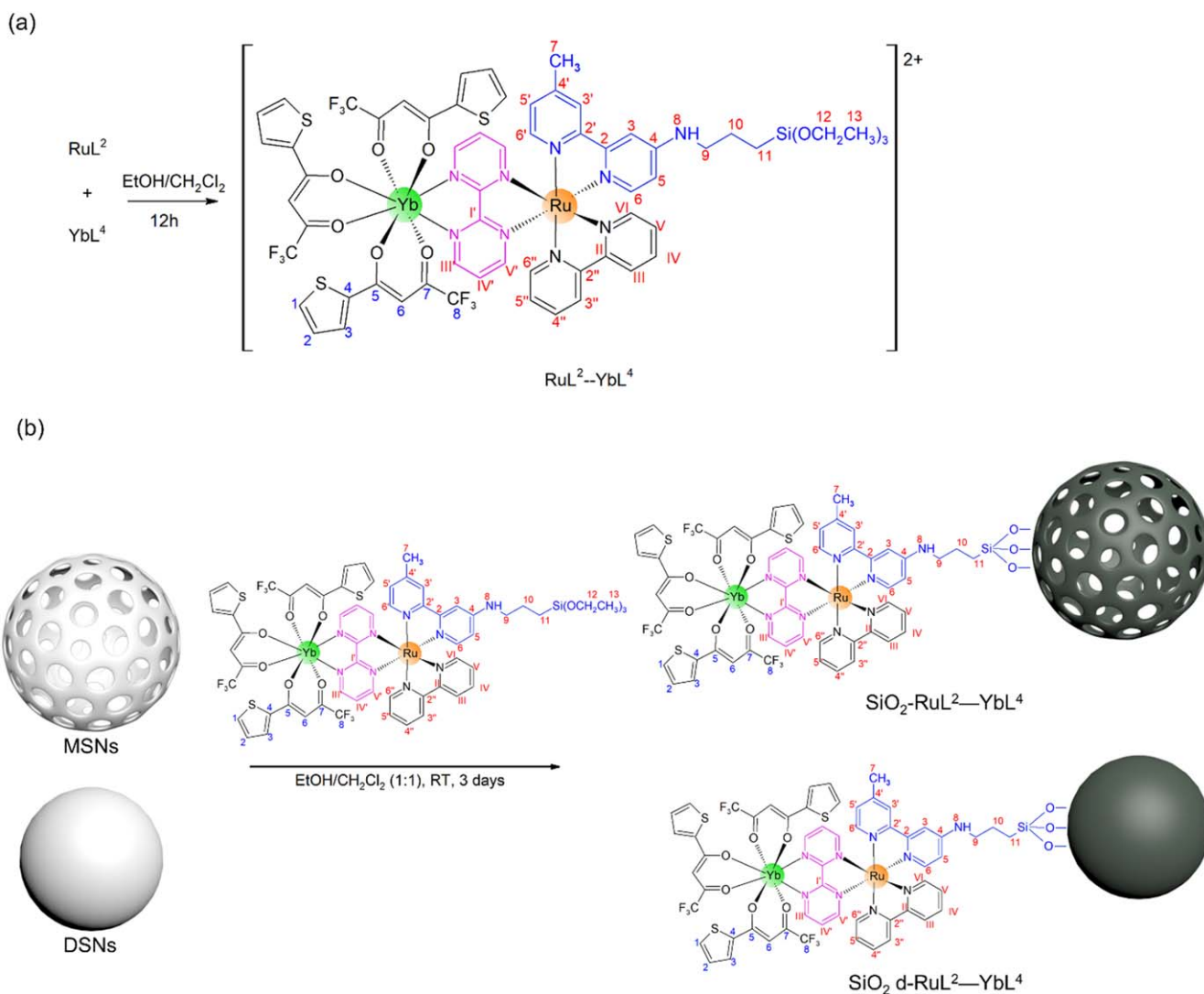
By equimolar reaction of RuL² complex with LnL⁴ (synthesis route and structure of RuL² and LnL⁴ are shown in figure S1, available online at stacks.iop.org/NANO/31/085709/mmedia), the synthesis of *df* heterobinuclear RuL² YbL⁴ complex was successfully performed as shown in Scheme 1(a). Structural characterization by EA, MS, FT-RAMAN, FTIR, 1D and 2D NMR are presented in details on support information.

Scheme 1(b) shows the fabrication of luminescent silica-based nanohybrids by grafting of the RuL² YbL⁴ complex onto MSNs or DSNs (labeled SiO₂-RuL² YbL⁴ and SiO₂d-RuL² YbL⁴, respectively). The grafting reactions are based on the establishment of covalent bounds between the complex and silica matrix by hydrolysis and condensation processes of the alkoxysilane groups onto the silanol groups available in the silica matrix.

¹³C{¹H}CP-MAS NMR analysis (figure 1(I)) were performed to confirm the chemical integrity of RuL² YbL⁴ complex. For SiO₂-RuL² YbL⁴ and SiO₂ d-RuL² YbL⁴, only signals ascribed to the ruthenium silylated complexes

were observed. The signals relating to the betadiketone ligands were not detected due to the paramagnetic interactions from ytterbium ions, compromising the efficiency of the cross-polarization process owing to very short ¹H spin-lattice relaxation times in the rotating frame [24]. The spectra present in figures 1(I) (a) and (b) were similar, showing signals at 162.5 (CIII'; IV'), 157.5 (CII; 2; 2'), 151.5 (C4; 4'; VI; 6; 6'), 138 (CIV) and 125.5 (CV; V'; 5; 5'; III; 3; 3') ppm assigned to the carbon atoms of the bpy and bpmd ligands. Signals at 58 (C8), 51.5 (C9), 21.5 (C10; 7) and 10 (C11) ppm were attributed to the ethoxysilyl groups present in the RuL² YbL⁴ complex. ²⁹Si{¹H}CP-MAS NMR measurements were carried out to confirm the grafting of the binuclear complexes onto the MSNs and DSNs. The covalent bond of the alkoxysilyl groups with the silanol available in the matrix can be confirmed by *Tⁿ* peaks usually observed from -55 to -70 ppm. ²⁹Si{¹H}CP-MAS NMR spectra from SiO₂-RuL² YbL⁴ and SiO₂ d-RuL² YbL⁴ nanohybrids (figures 1(II), (a) and (b), respectively) show *T²* and *T³* peaks at -59, -68 and -59, -67 ppm, respectively, attributed to the covalent bond of ethoxysilyl groups onto MSNs and DSNs. Results confirm the condensation of the ethoxysilyl and methoxysilyl groups present in the complexes with the silanol available in the MSNs and DSNs. These results are in agreement with DRIFT analysis (figure S11) confirming the chemical integrity and grafting of the RuL² YbL⁴ complexes in both nanosystems.

Figure 2 shows STEM images (A1 and A6) and elemental mapping of the Si (A2), Yb (A3), Ru (A4) atoms and all of them superposed (A5) for SiO₂-RuL² YbL⁴ nanohybrid. Figure 2(A1) suggests homogeneous distribution of the metallic atoms onto MSNs and the elemental mapping of Si atoms (figure 2(A2)) shows their homogenous distribution to form MSNs. Elemental mapping of Yb and Ru atoms (figures A3 and A4, respectively) confirm their homogeneously dispersion onto MSNs surface. The elemental mapping obtained by Si, Yb and Ru overlay (figure 2(A5)) corroborate high concentration and homogeneous distribution of Yb and Ru atoms inside the nanopores of MSNs. Figure 2(B6) shows the distribution profile of Ru and Yb atoms with similar concentration of both inside the MSNs nanopores. These results are in agreement with notable grafting ratios of 0.13 and 0.13 mmol g⁻¹ of silica, for Ru(II) and Yb(III) moieties, respectively, obtained from EA data (table 1). The SiO₂ d-RuL² YbL⁴ nanohybrid displayed similar results from STEM measurements with homogeneous distribution of the metallic atoms onto DSNs (figure 2(B1)) and elemental mapping of Si atoms (figure 2(B2)) exhibiting that the morphology and structure of DSNs were kept intact. Elemental mapping of Yb and Ru atoms (figures 2(A3) and (A4), respectively) displays both elements well dispersed onto DSNs. Despite homogeneous distribution of Yb and Ru onto DSNs surface detected, figure 2(A5) suggests low concentration of Yb and Ru onto DSNs surface. These results are consistent with the distribution profile (figure 2(B6)) that shows low and similar concentration of both metallic atoms. It is worth emphasizing that low grafting efficiencies were obtained due to low ratios of RuL² YbL⁴ complex



Scheme 1. Synthesis of the $\text{RuL}^2\text{-YbL}^4$ heterobinuclear complex (a) and fabrication of luminescent nanohybrids by grafting of the $\text{RuL}^2\text{-YbL}^4$ onto MSNs (labeled $\text{SiO}_2\text{-RuL}^2\text{-YbL}^4$) and DSNs ($\text{SiO}_2\text{ d-RuL}^2\text{-YbL}^4$). Numbering of the hydrogen and carbon atoms are identified as red and blue labels.

(0.06 mmol g^{-1} of silica) added to the DSNs. STEM results corroborate grafting efficiencies of 0.04 and 0.04 mmol g^{-1} of silica for Ru(II) and Yb(III) moieties, respectively, detected by EA analysis (table 1).

Coherent values of grafting efficiencies confirm the remarkable results obtained by STEM and EA analysis. Grafting efficiency was higher for MSNs than DSNs due to the specific surface area of 765 $\text{m}^2 \text{g}^{-1}$ for MSNs whereas DSNs present 138 $\text{m}^2 \text{g}^{-1}$ of silica [17, 20].

The grafting efficiencies of the $\text{RuL}^2\text{-YbL}^4$ complex were calculated according to the N and S contents as previously described [17, 18, 21, 25]. Table 1 displays grafting efficiencies, R, in mmol of ruthenium and lanthanide complexes g^{-1} of silica and amount of binuclear complexes nm^{-2} of silica for the nanohybrids.

The number of complexes per nm^2 grafted onto MSNs were lower than from DSNs (0.12 and 0.17 complex nm^{-2} , respectively). This difference can be attributed to the silanol

groups, which are more available in DSNs than in MSNs. Additionally, MSNs were submitted to heat treatment whereas DSNs are used directly for grafting reactions without any treatment.

3.2. Luminescent properties

By monitoring the luminescence properties of Ru(II) moieties in the nanohybrids the emission levels were determined as shown in figures 3(a1) and (b1). A broad emission band was observed and it can be ascribed to the Ru(II) $^3\text{MLCT}$ emission to the ground state [19, 26] at 610 and 614 nm for $\text{SiO}_2\text{-RuL}^2\text{-YbL}^4$ and $\text{SiO}_2\text{ d-RuL}^2\text{-YbL}^4$, respectively. The excitation spectra for both nanohybrids, obtained by monitoring the Ru(II) $^3\text{MLCT}$ emission, show bands assigned to the $d \rightarrow \pi^*$ $^1\text{MLCT}$ (MLCT) transitions and transitions centered on ligands, as $\pi \rightarrow \pi^*$ transitions [19, 26]. Both

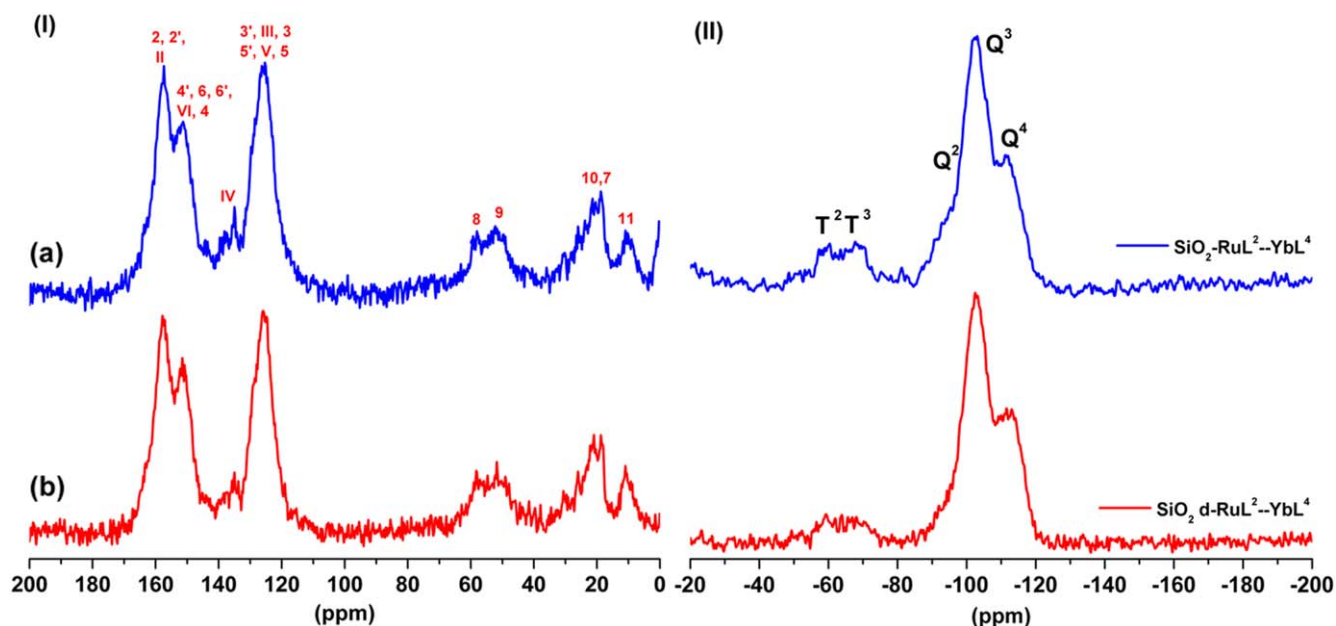


Figure 1. $^{13}\text{C}\{^1\text{H}\}$ CP MAS NMR spectra (I) and $^{29}\text{Si}\{^1\text{H}\}$ CP MAS NMR spectra (II) of (a) $\text{SiO}_2\text{-RuL}^2\text{-YbL}^4$ and (b) $\text{SiO}_2\text{ d-RuL}^2\text{-YbL}^4$.

emission and excitation spectra are in agreement with the respective free $\text{RuL}^2\text{-YbL}^4$ complex (figure S9).

By monitoring the NIR emission (λ_{em} : 980 and 979 nm for $\text{SiO}_2\text{-RuL}^2\text{-YbL}^4$ and $\text{SiO}_2\text{ d-RuL}^2\text{-YbL}^4$, respectively), the excitation spectra have shown distinct profile. For the $\text{SiO}_2\text{-RuL}^2\text{-YbL}^4$ nanohybrid, the excitation spectrum (figure 3(a3)) displays a broad excitation band from 270 to 400 nm assigned to ligands transitions (TTA, bpy-Si and bpm) [17, 21, 27, 28]. Bands above 400 nm were ascribed to Ru(II) $^3\text{MLCT}$ transition [19, 26]. The emission spectra (figure 3(a4)) display similar profiles relating to the free $\text{RuL}^2\text{-YbL}^4$ complex. By monitoring the excitation up to 400 nm, the broad emission bands observed at 980 nm were ascribed to Yb(III) $^2\text{F}_{5/2} \rightarrow ^2\text{F}_{7/2}$ transitions [19, 26, 29, 30]. It is worth emphasizing that monitoring excitation up to 400 nm a split of $^2\text{F}_{5/2} \rightarrow ^2\text{F}_{7/2}$ transitions could be detected as exhibited in figure 3(a4), red line). When the excitation was monitoring on the Ru(II) $^1\text{MLCT}$ transition (above 400 nm), the IR emission spectra was observed and assigned to the same transition but displaying distinct profile as depicted in figure 3(a4), black line).

For the $\text{SiO}_2\text{ d-RuL}^2\text{-YbL}^4$ nanohybrid, the excitation spectrum (figure 3(b3)) displays a broad band at 345 nm resulting from ligands transitions (TTA, bpy-Si and bpm) [17, 21, 27, 28] and a low intensity band above 400 nm assigned to the Ru(II) $^3\text{MLCT}$ transitions [19, 26]. By monitoring the excitation up to 400 nm, the broad emission bands (figure 3(b4)) centered at 979 nm were ascribed to Yb(III) $^2\text{F}_{5/2} \rightarrow ^2\text{F}_{7/2}$ transitions [19, 26, 29, 30]. When the excitation was monitored on the Ru(II) $^1\text{MLCT}$ transition, the similar broad band was also detected [19, 26, 29, 30]. Finally, the approach by using a heterobinuclear complex instead of an equimolar mixture of the two individual complexes was important evolution for biological applications (in following),

because in this paper the efficiency of energy transfer in $\text{RuL}^2\text{-YbL}^4$ complex was 73.4% (see table S2), a higher value regarding to previous studies [31]. The presence of a bridge ligand (2,2'-bipyrimidine) that can favor the communication and, consequently, efficient energy transfer from Ru(II) moieties to near-infrared lanthanide(III) ions.

3.3. Cytotoxicity assays

3.3.1. Cell viability. In order to evaluate the potential of the nanohybrid to be employed as nanomarkers in biological samples, their cytotoxicity was evaluated in *in vitro* assays using healthy and cancer cells. When fibroblast (HDFn) and melanoma (B16-F10) cell lines were exposed to a wide range of $\text{SiO}_2\text{-RuL}^2\text{-YbL}^4$ nanohybrid concentrations, a dose-dependent behavior of cell viability was observed, with higher sample concentrations resulting in more expressive viability loss (figure 4). However, time exposure does not seem to affect extensively cell survival in the evaluated period. Mild and slight cytotoxicity was verified in B16-F10 cells when $50\ \mu\text{g ml}^{-1}$ were used, with viability values remaining close to 73% and 89% for 24 and 48 h, respectively. Notwithstanding, moderate cell death was promoted by increasing five times $\text{SiO}_2\text{-RuL}^2\text{-YbL}^4$ nanohybrid concentration resulting in 59% and 68% of viable cells after 24 and 48 h of incubation, respectively. Exposure of the healthy cell line to the same experimental conditions promoted mild cytotoxicity in low concentrations, suggesting this cell line has a higher susceptibility to cell damage than the previous cells: viability values of approximately 61% and 69% were obtained after 24 and 48 h of $50\ \mu\text{g ml}^{-1}$ solutions incubation. Despite the apparent susceptibility of fibroblasts to $\text{SiO}_2\text{-RuL}^2\text{-YbL}^4$ nanohybrid, the substantial increase on its concentration did not result in

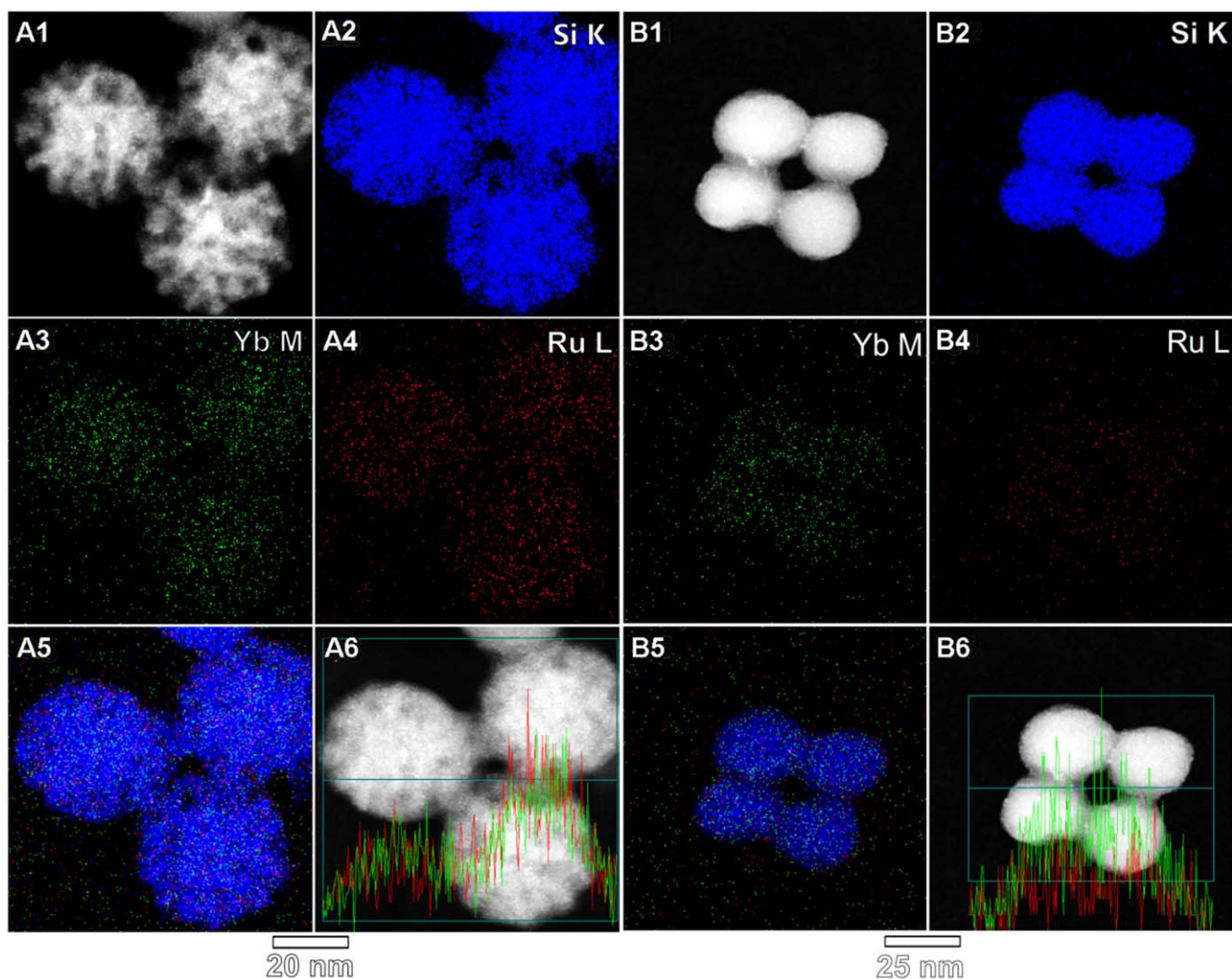


Figure 2. Electron microscope images and elemental mapping of the (A) $\text{SiO}_2 \text{RuL}^2 \text{YbL}^4$ and (B) $\text{SiO}_2 \text{d RuL}^2 \text{YbL}^4$: (A1 and B1) STEM images, (A2 and B2) Si mapping, (A3 and B3) Yb mapping, (A4 and B4) Ru mapping, (A5 and B5) Si (blue color), Ru (red color) and Yb (green color) mapping. (A6 and B6) STEM image with a line profile of Ru (red line) and Yb (green line) atoms in the selected area (blue line).

Table 1. Grafting efficiencies, in mmol of ruthenium and lanthanide complexes g^{-1} of silica, and amount of heterobinuclear complexes nm^{-2} of silica for the nano hybrids.

Samples	From elemental analysis (mmol of complex per g of SiO_2)		Number of binuclear complex per nm^2
	R_{Ru}	R_{Yb}	
$\text{SiO}_2 \text{RuL}^2 \text{YbL}^4$	0.13	0.13	0.12
$\text{SiO}_2 \text{d RuL}^2 \text{YbL}^4$	0.04	0.04	0.17

greater viability loss when HDFn cells are compared to B16-F10 cells: the lowest viability values were produced using $250 \mu\text{g ml}^{-1}$ solutions (approximately 59% for both incubation times). To study the influence of time exposure and susceptibility of each cell line to the nanoparticles, IC50 values (half maximum inhibitory concentration) were determined using a nonlinear regression in GraphPad Prism

5: 507.7 and $400.2 \mu\text{g ml}^{-1}$ for B16-F10 cells after $\text{SiO}_2\text{-RuL}^2 \text{YbL}^4$ incubation for 24 and 48 h, respectively, and $365.9 \mu\text{g ml}^{-1}$ after 48 h for HDFn cells (for 24 h, it was not possible to determine this parameter due the absence of convergence). The decrease on IC50 values over time for B16-F10 cells indicates that longer exposure times have a negative impact on cell viability. The comparison of HDFn cells IC50 to the melanoma cells also indicates that the healthy cell line is slightly more prone to cell damage caused by $\text{SiO}_2\text{-RuL}^2 \text{YbL}^4$ nano hybrid.

Lanthanides have been explored to dope luminescent nanoparticles due their interesting chemical and optical properties. Although these elements are considered relatively non-toxic, nanomaterials possess a high surface-to-volume ratio, what might interfere in its biocompatibility. Therefore, cytotoxic effects of lanthanide-doped nanoparticles assessed in *in vitro* models provide helpful information for nanotoxicity prediction, especially due the wide variety of nanoparticles synthesis and cytotoxicity reported by the scientific

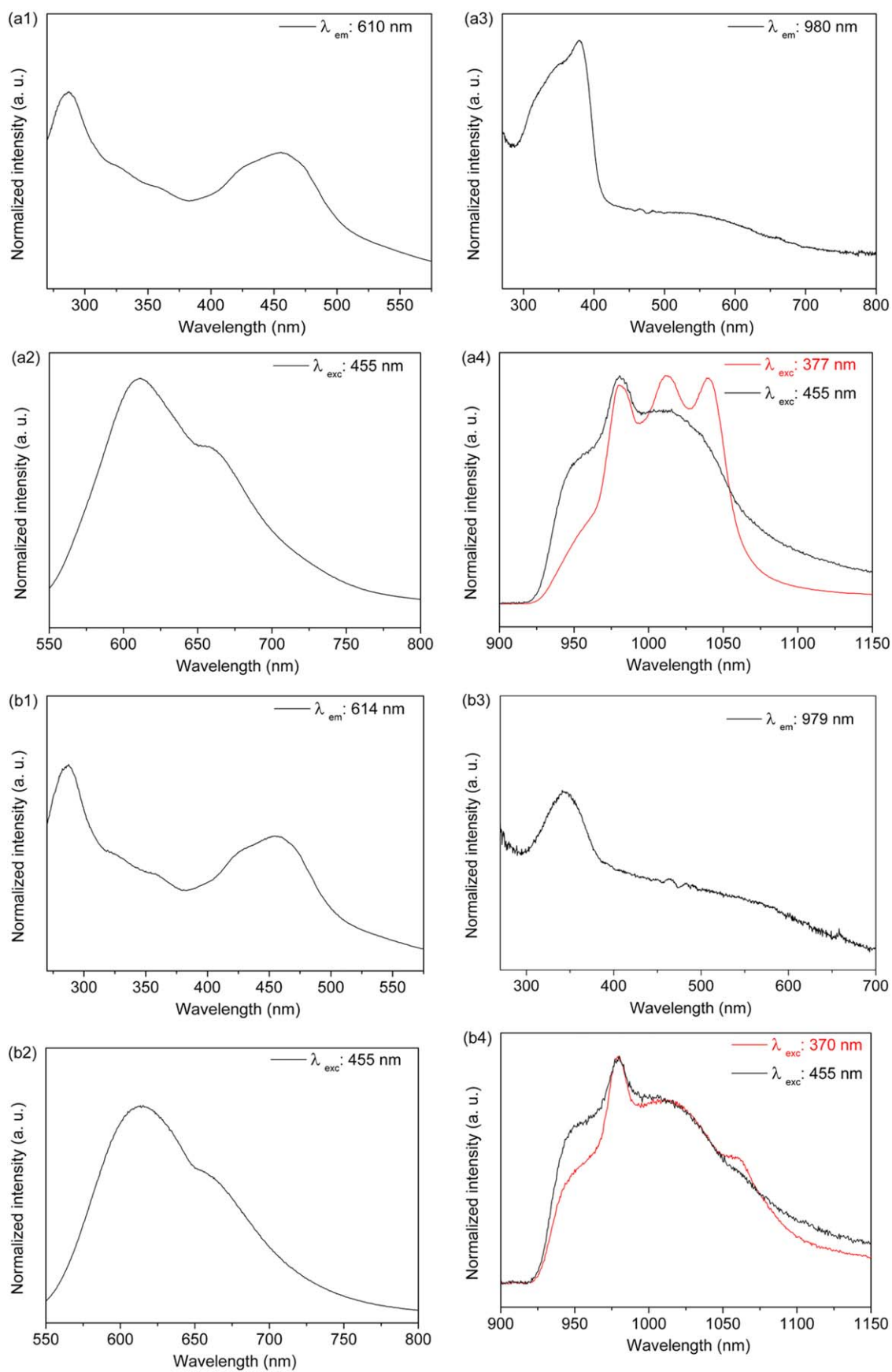


Figure 3. Room temperature excitation ((a1), $\lambda_{\text{emission}}$: 610 nm; (a3), $\lambda_{\text{emission}}$: 980 nm; (b1), $\lambda_{\text{emission}}$: 614 nm; (b3), $\lambda_{\text{emission}}$: 979 nm) and emission ((a2), $\lambda_{\text{excitation}}$: 455 nm; (a4), $\lambda_{\text{excitation}}$: 377 and 455 nm); (b2), $\lambda_{\text{excitation}}$: 455 nm; (b4), $\lambda_{\text{excitation}}$: 370 and 455 nm) spectra of the (a) $\text{SiO}_2/\text{RuL}^2/\text{YbL}^4$ and (b) $\text{SiO}_2 \text{ d } \text{RuL}^2/\text{YbL}^4$ nanohybrids in solid state.

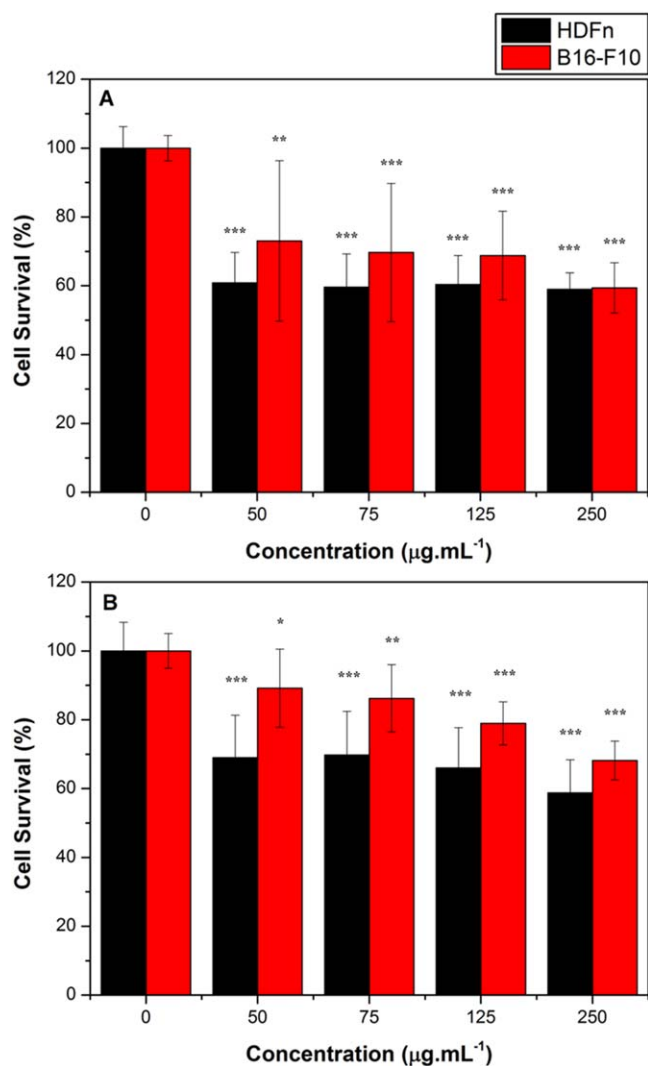


Figure 4. Cytotoxicity evaluation in HDFn and B16 F10 cells with varying concentration of $\text{SiO}_2\text{-RuL}^2\text{-YbL}^4$. Samples were incubated for (A) 24 and (B) 48 h. The symbols *, ** and *** represent groups that have significant statistical differences ($p \leq 0.05$, 0.005 and 0.0005, respectively) when compared to the control group (not exposed to $\text{SiO}_2\text{-RuL}^2\text{-YbL}^4$ nanohybrid).

community [32]. To our best knowledge, the presented nanohybrid has not yet been described, however their cytotoxicity can be compared to the one produced by other lanthanide-doped systems. Fedorenko *et al* [33] reported two Tb(III)-doped aminomodified silica nanoparticles of 20 and 35 nm and evaluated, after 72 h of incubation, their cytotoxicity in human larynx carcinoma cell line. While the 35 nm presented no cytotoxic effects, 150 $\mu\text{g ml}^{-1}$ solution of the smaller nanoparticles induced approximately 50% of cell death (IC50: 161 $\mu\text{g ml}^{-1}$). Osseni *et al* [34] described gadolinium oxysulfide nanoparticles doped with Yb^{3+} , Er^{3+} and Eu^{3+} , assessing cytotoxicity in triple negative breast cancer cell line with 0.1 2 mg ml⁻¹ for 24 and 72 h [34]. After 72 h exposure, viability loss of approximately 30% was observed. Wozniak *et al* [35] studied the effects of $\beta\text{-NaGdF}_4\text{:Yb}^{3+}\text{Er}^{3+}$ nanorods coated with polyethylene glycol monooleate in human colorectal cancer, human

cervical cancer, human bone osteosarcoma and normal human embryonic kidney cell lines [35]. Concentrations of 1 300 $\mu\text{g ml}^{-1}$ were incubated for 24, 48 and 72 h, revealing that, overall, osteosarcoma, cervical cancer and embryonic kidney cell lines were more susceptible to nanoparticles cytotoxic effects, especially when 300 $\mu\text{g ml}^{-1}$ solutions were used (resulting in <40% of cell survival).

3.4. Bioimaging applications

3.4.1. Nanoparticles uptake and intracellular distribution. To verify $\text{SiO}_2\text{-RuL}^2\text{-YbL}^4$ nanohybrid internalization, LSCM was performed. One-photon and two-photon excitation results can be observed (figures 5 and 6) for both cell lines when incubated with 50 and 250 $\mu\text{g ml}^{-1}$ for 24 h. The presence of aggregates is verified in both concentrations despite the use of ultrasound to prepare the samples, most likely due the chosen FBS concentration promoting a corona formation [36]. However, the aggregates were co-localized with cells, what suggests the nanoparticles interact with cell membranes. It is possible to observe the overlay of fluorescence with the cell cytoplasm and the lack of fluorescence around a round portion inside the cells, a strong indication that $\text{SiO}_2\text{-RuL}^2\text{-YbL}^4$ nanohybrids are internalized by the healthy and tumor cells over 24 and 48 h, but remain outside the nucleus. Two-photon images show a clear fluorescence signal, even for lower nanoparticles concentration.

In order to confirm the nanoparticle uptake, flow cytometry was used to observe the fluorescence signal of cells suspensions when they were incubated with the nanohybrids as shown in figure 7. For both incubation times, when the fluorescence signal produced by the negative control (cells that were not exposed to nanoparticles) is compared to the one produced by cells incubated with 50 and 250 $\mu\text{g ml}^{-1}$, a shift on cell population towards augmented fluorescence is observed, revealing that cells have stronger fluorescence when they are exposed to the nanohybrids. This indicates both cell lines have successfully internalized the nanoparticles. The increase on $\text{SiO}_2\text{-RuL}^2\text{-YbL}^4$ nanohybrids concentration results in a shift on cell population towards stronger fluorescence intensity signal, indicating that more cells internalized increasing amounts of nanoparticles.

These results show that, despite the $\text{SiO}_2\text{-RuL}^2\text{-YbL}^4$ nanohybrids aggregation in cell media, both cell lines internalize the nanostructures in a dose-dependent manner. The interaction with cell membrane, which might interfere in its function and the presence of higher quantities of nanoparticles in the cytoplasm, may result in the cell survival reduction that was observed for the 250 $\mu\text{g ml}^{-1}$ solution. Lower concentrations of the nanoparticles resulted in a greater number of viable cells and produced an intense fluorescence signal for both one and two-photon excitation, indicating that $\text{SiO}_2\text{-RuL}^2\text{-YbL}^4$ nanohybrid has great potential to be used as a dual-emitting visible and NIR activated biomarker.

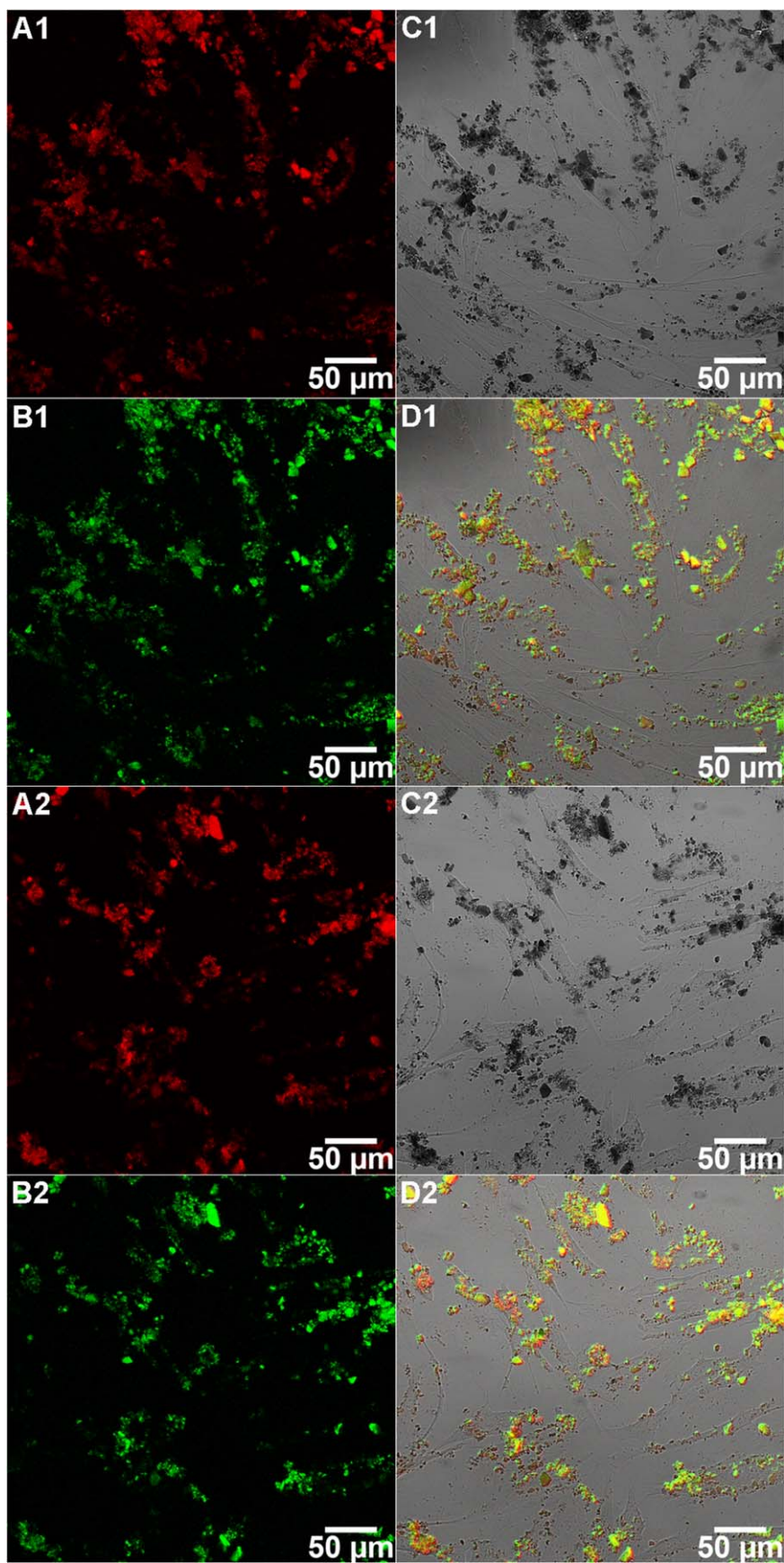


Figure 5. One photon (A) and two photon (B) excitation of $\text{SiO}_2 \text{RuL}^2 \text{YbL}^4$ nanoparticles, with phase contrast (C) and merge image (D) of HDFn cells exposed for 24 h to 50 (A1 D1) and 250 (A2 D2) $\mu\text{g ml}^{-1}$.

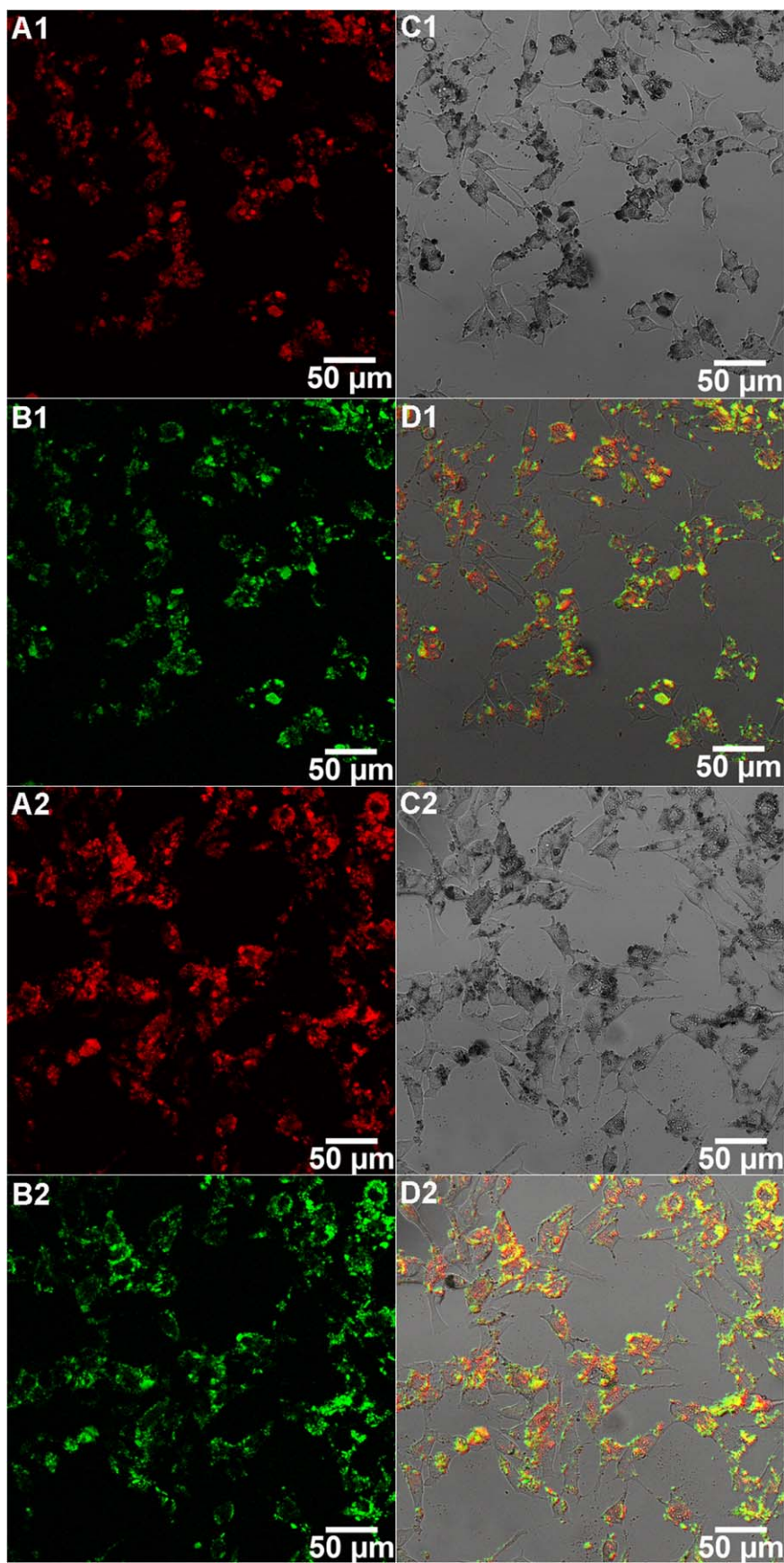


Figure 6. One photon (A) and two photon (B) excitation of $\text{SiO}_2 \text{RuL}^2 \text{YbL}^4$ nanoparticles, with phase contrast (C) and merge image (D) of B16 F10 cells exposed for 24 h to 50 (A1 D1) and 250 (A2 D2) $\mu\text{g ml}^{-1}$.

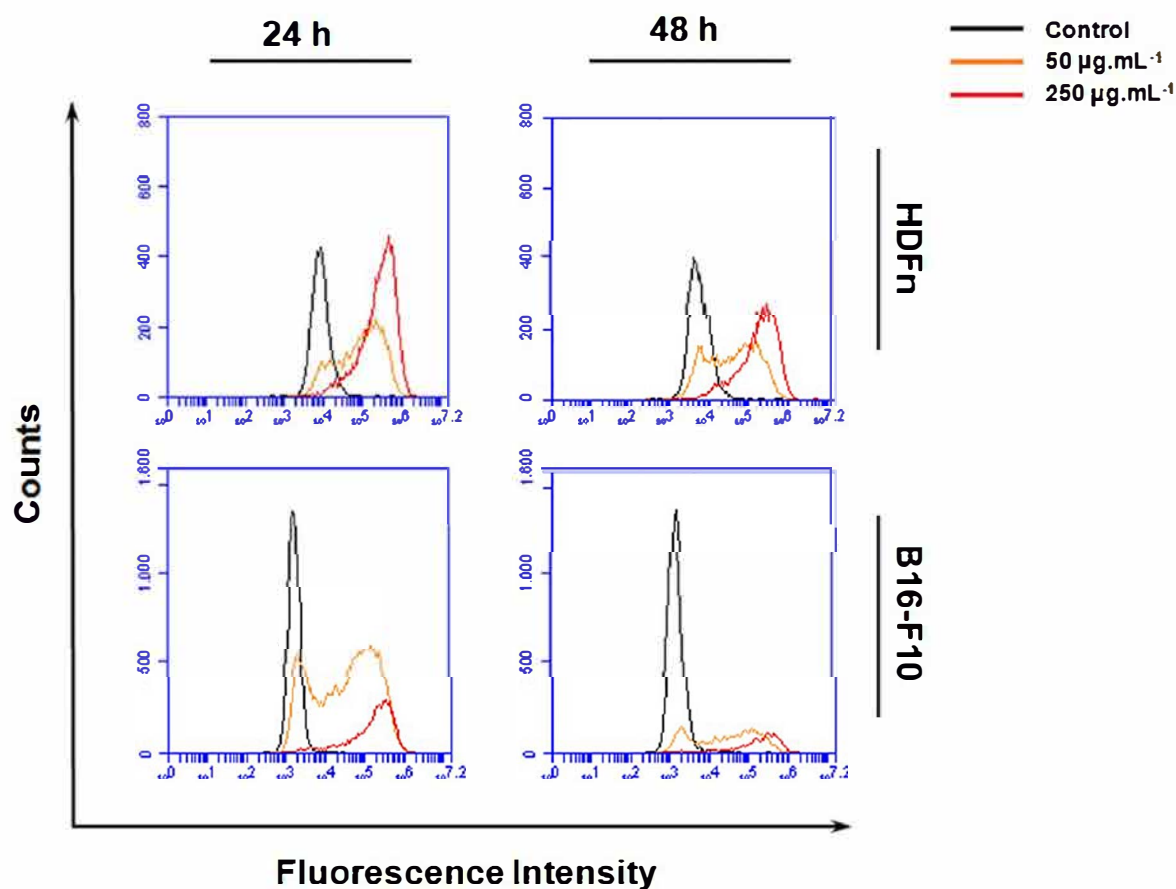


Figure 7. Uptake of nanoparticles in HDFn (upper row) and B16 F10 (bottom row) cells after 24 (left column) and 48 h (right column) of incubation. The negative control histogram is displayed in black, while cells incubated with 50 and 250 $\mu\text{g mL}^{-1}$ are displayed in orange and red, respectively.

4. Conclusion

New luminescent silica-based nanohybrids were designed by grafting of silylated Ru(II) Yb(III) heterobinuclear complex onto DSNs and MSNs. The luminescent nanohybrids labeled $\text{SiO}_2\text{-RuL}^2\text{ YbL}^4$ and $\text{SiO}_2\text{ d-RuL}^2\text{ YbL}^4$ were structurally characterized by DRIFT, solid-state NMR, EA, STEM measurements. $^{13}\text{C}\{^1\text{H}\}$ CP-MAS NMR results exhibits the $\text{RuL}^2\text{ YbL}^4$ chemical integrity as well as DRIFT, EA and $^{29}\text{Si}\{^1\text{H}\}$ CP-MAS NMR confirm the $\text{RuL}^2\text{ YbL}^4$ grafting onto silica matrices. Elemental mapping from STEM analysis displays the homogeneously distribution of ruthenium and ytterbium elements onto silica surface. Luminescence properties of these nanohybrids were explored by monitoring the excitation onto Ru(II) moieties and compared to the corresponding free $\text{RuL}^2\text{ YbL}^4$ complex. Visible/NIR-emitting nanohybrids were successfully fabricated according to the luminescent results. The $\text{SiO}_2\text{-RuL}^2\text{ YbL}^4$ nanohybrid showed low cytotoxicity to fibroblasts and murine melanoma cells in *in vitro* assays, where a closed system was evaluated, with no homeostasis to fight disturbances inserted in the biological model. The nanohybrid was efficiently internalized by both cell lines over 24 and 48 h, presenting good fluorescence signal for both one and two-photon excitation, strongly suggesting the presented material is a promising candidate to be used as a biomarker.

Acknowledgments

This work was supported by the Brazilian agencies FAPESP, CNPq, CAPES and CAPES-COFECUB Brazil-France cooperation program for Grant to R M Sábio.

ORCID iDs

Rafael Miguel Sábio  <https://orcid.org/0000-0002-3852-2184>

Robson Rosa da Silva  <https://orcid.org/0000-0001-6887-4749>

References

- [1] Kaczmarek M T, Zabizak M, Nowak M and Jastrzab R 2018 Lanthanides: Schiff base complexes, applications in cancer diagnosis, therapy, and antibacterial activity *Coord. Chem. Rev.* **370** 42–54
- [2] Lo W S, Li H, Law G L, Wong W T and Wong K L 2016 Efficient and selective singlet oxygen sensitized NIR luminescence of a neodymium(III) complex and its application in biological imaging *J. Lumin.* **169** 549–52

- [3] Chen F F, Chen Z Q, Bian Z Q and Huang C H 2010 Sensitized luminescence from lanthanides in d f bimetallic complexes *Coord. Chem. Rev.* **254** 991 1010
- [4] Bünzli J C G 2016 Lanthanide light for biology and medical diagnosis *J. Lumin.* **170** 866 78
- [5] Chen Y, Guan R, Zhang C, Huang J, Ji L and Chao H 2016 Two photon luminescent metal complexes for bioimaging and cancer phototherapy *Coord. Chem. Rev.* **310** 16 40
- [6] Xu W, Zuo J, Wang L, Ji L and Chao H 2014 Dinuclear ruthenium(II) polypyridyl complexes as single and two photon luminescence cellular imaging probes *Chem. Commun.* **50** 2123
- [7] Baggaley E, Gill M R, Green N H, Turton D, Sazanovich I V, Botchway S W, Smythe C, Haycock J W, Weinstein J A and Thomas J A 2014 Dinuclear ruthenium(II) complexes as two photon, time resolved emission microscopy probes for cellular DNA *Angew. Chem. Int. Ed.* **53** 3367 71
- [8] Sykes D, Tidmarsh I S, Barbieri A, Sazanovich I V, Weinstein J A and Ward M D 2011 d → f energy transfer in a series of Ir^{III}/Eu^{III} dyads: energy transfer mechanisms and white light emission *Inorg. Chem.* **50** 11323 39
- [9] Ward M D 2007 Transition metal sensitised near infrared luminescence from lanthanides in d f heteronuclear arrays *Coord. Chem. Rev.* **251** 1663 77
- [10] Lazarides T, Sykes D, Faulkner S, Barbieri A and Ward M D 2008 On the mechanism of d f energy transfer in RuII/LnIII and OsII/LnIII Dyads: Dexter type energy transfer over a distance of 20 Å *Chem. Eur. J.* **14** 9389 99
- [11] Lazarides T, Tart N M, Sykes D, Faulkner S, Barbieri A and Ward M D 2009 [Ru(bipy)₃]²⁺ and [Os(bipy)₃]²⁺ chromophores as sensitizers for near infrared luminescence from Yb(III) and Nd(III) in d/f dyads: contributions from Förster, Dexter, and redox based energy transfer mechanisms *Dalt. Trans.* 3971 9
- [12] Wei Q H, Lei Y F, Xu W R, Xie J M and Chen G N 2012 Ru (II) sensitized lanthanide luminescence: synthesis, photophysical properties, and near infrared luminescent determination of alpha fetal protein (AFP) *Dalt. Trans.* **41** 11219
- [13] Coti K K, Belowich M E, Liong M, Ambrogio M W, Lau Y A, Khatib H A, Zink J I, Khashab N M and Stoddart J F 2009 Mechanised nanoparticles for drug delivery *Nanoscale* **1** 16
- [14] Fadeel B and Garcia Bennett A E 2010 Better safe than sorry: understanding the toxicological properties of inorganic nanoparticles manufactured for biomedical applications *Adv. Drug Deliv. Rev.* **62** 362 74
- [15] Sábio R M, Meneguín A B, Ribeiro T C, Silva R R and Chorilli M 2019 New insights towards mesoporous silica nanoparticles as a technological platform for chemotherapeutic drugs delivery *Int. J. Pharm.* **564** 379 409
- [16] Cousinié S, Gressier M, Alphonse P and Menu M J 2007 Silica based nanohybrids containing dipyridine, urethan, or urea derivatives *Chem. Mater.* **19** 6492 503
- [17] Duarte A P, Gressier M, Menu M J, Dexpert Ghys J, Caiut J M A and Ribeiro S J L 2012 Structural and luminescence properties of silica based hybrids containing new silylated diketonato europium(III) complex *J. Phys. Chem. C* **116** 505 15
- [18] Sábio R M, Gressier M, Caiut J M A, Menu M J and Ribeiro S J L 2016 Luminescent multifunctional hybrids obtained by grafting of ruthenium complexes on mesoporous silica *Mater. Lett.* **174** 1 5
- [19] Sábio R M, Santagneli S H, Gressier M, Caiut J M A, Pazin W M, Silva R R, Ribeiro S J L and Menu M J 2019 Near infrared luminescence from visible light sensitized ruthenium(II) neodymium(III) heterobimetallic bridged complexes containing alkoxy(silyl) functional groups *J. Braz. Chem. Soc.* (<https://doi.org/10.21577/01035053.20190233>)
- [20] Duarte A P *et al* 2013 Organosilylated complex [Eu(TTA)₃(Bpy Si)]: a bifunctional moiety for the engineering of luminescent silica based nanoparticles for bioimaging *Langmuir* **29** 5878 88
- [21] Cousinié S, Mauline L, Gressier M, Kandibanda S R, Datas L, Reber C and Menu M J 2012 Bulk or surface grafted silylated Ru(II) complexes on silica as luminescent nanomaterials *New J. Chem.* **36** 1355
- [22] Mauline L, Gressier M, Roques C, Hammer P, Ribeiro S J L, Caiut J M A and Menu M J 2013 Bifunctional silica nanoparticles for the exploration of biofilms of *Pseudomonas aeruginosa* *Biofouling* **29** 775 88
- [23] Nandiyanto A B D, Kim S G, Iskandar F and Okuyama K 2009 Synthesis of spherical mesoporous silica nanoparticles with nanometer size controllable pores and outer diameters *Microporous Mesoporous Mater.* **120** 447 53
- [24] Ilibi M, de Queiroz T B, Ren J, De Cola L, de Camargo A S S and Eckert H 2014 Luminescent hybrid materials based on covalent attachment of Eu(III) tris (bipyridinedicarboxylate) in the mesoporous silica host MCM 41 *Dalt. Trans.* **43** 8318 30
- [25] Cousinié S, Gressier M, Reber C, Dexpert Ghys J and Menu M J 2008 Europium(III) complexes containing organosilyldipyridine ligands grafted on silica nanoparticles *Langmuir* **24** 6208 14
- [26] Zhang L Y, Hou Y J, Pan M, Chen L, Zhu Y X, Yin S Y, Shao G and Su C Y 2015 Near infrared (NIR) emitting Nd/Yb(III) complexes sensitized by MLCT states of Ru(II)/Ir (III) metalloligands in the visible light region *Dalt. Trans.* **44** 15212 9
- [27] Fratini A, Richards G, Larder E and Swavey S 2008 Neodymium, gadolinium, and terbium complexes containing hexafluoroacetylacetonate and 2,2' bipyrimidine: structural and spectroscopic characterization *Inorg. Chem.* **47** 1030 6
- [28] Zucchi G, Maury O, Thuéry P and Ephritikhine M 2008 Structural diversity in neodymium bipyrimidine compounds with near infrared luminescence: from mono and binuclear complexes to metal organic frameworks *Inorg. Chem.* **47** 10398 406
- [29] Singaravadi S, Babu E, Velayudham M, Lu K L and Rajagopal S 2013 Sensitized near infrared luminescence of Nd(III), Yb(III) and Er(III) complexes by energy transfer from a ruthenium antenna *J. Organomet. Chem.* **738** 49 54
- [30] Martín Ramos P, Pereira da Silva P S, Lavín V, Martín I R, Lahoz F, Chamorro Posada P, Ramos Silva M and Martín Gil J 2013 Structure and NIR luminescence of ytterbium(III) beta diketonato complexes with 5 nitro 1,10 phenanthroline ancillary ligand: assessment of chain length and fluorination impact *Dalt. Trans.* **42** 13516
- [31] Sábio R M, Santagneli S H, Gressier M, Caiut J M A, Pazin W M, Ribeiro S J L and Menu M J 2019 Near infrared/visible emitting nanosilica modified with silylated Ru(II) and Ln(III) complexes *Nanotechnology* **31** 035602
- [32] Gnach A, Lipinski T, Bednarkiewicz A, Rybka J and Capobianco J A 2015 Upconverting nanoparticles: assessing the toxicity *Chem. Soc. Rev.* **44** 1561 84
- [33] Fedorenko S V *et al* 2017 Cellular imaging by green luminescence of Tb(III) doped aminomodified silica nanoparticles *Mater. Sci. Eng. C* **76** 551 8
- [34] Osseni S A *et al* 2014 Gadolinium oxysulfide nanoparticles as multimodal imaging agents for T₂ weighted MR, x ray tomography and photoluminescence *Nanoscale* **6** 555 64
- [35] Woźniak A *et al* 2016 Cytotoxicity and imaging studies of β NaGdF₄:Yb³⁺Er³⁺ @PEG Mo nanorods *RSC Adv.* **6** 95633 43
- [36] Lesniak A, Fenaroli F, Monopoli M P, Åberg C, Dawson K A and Salvati A 2012 Effects of the presence or absence of a protein corona on silica nanoparticle uptake and impact on cells *ACS Nano* **6** 5845 57